On co-existing diffusive and anti-diffusive tracer transport by oceanic mesoscale eddies

Michael Haigh [a,*], Pavel Berloff [a,b]

[a] *Department of Mathematics, Imperial College London, London, United Kingdom*
[b] *Institute of Numerical Mathematics, Russian Academy of Sciences, Gubkina 8, 119333 Moscow, Russia*

ARTICLE INFO

ABSTRACT

A common approach for parameterising eddy transport of passive tracers by mesoscale eddies in the ocean is by invoking a transport tensor. The symmetric part of this tensor, the diffusion tensor, quantifies diffusive eddy tracer transport. Recent studies have diagnosed opposite-signed eigenvalues (diffusivities) of the diffusion tensor from eddy-resolving simulations, while all current parameterisations implement only positive diffusivities. For opposite-signed eigenvalues the associated diffusive eddy tracer flux is not necessarily down-gradient and therefore may not mix the tracer by transferring variance to the small scales. In this study we explore such diffusive eddy fluxes by using an eddy-resolving simulation of passive tracers with a relaxation (source/sink) forcing. After confirming that the diffusion tensors for different tracer pairs have opposite-signed eigenvalues, we show that the corresponding diffusive eddy tracer flux drives a net down-gradient transfer of variance, as would be guaranteed when the diffusion tensor eigenvalues are both positive. Locally up-gradient fluxes are common, with their frequency strongly dependent on the relaxation profile. The effects of weakening/strengthening the relaxation on the frequency of down-gradient fluxes is different for each tracer. However, for all tracers considered the amplitude of the net down-gradient transfer weakens as the relaxation strengthens, a consequence of the homogeneous diffusion dissipating less eddy variance. Our results indicate that for oceanic tracers with sources/sinks the parameterised diffusive eddy tracer fluxes should not be globally down-gradient.

1. Introduction

Mesoscale eddies make a leading-order contribution to the transport of passive tracers about the ocean, but computational limitations often dictate that eddy effects cannot be resolved in ocean circulation models. The current solution to this issue is to parameterise the missing eddy effects. Current parameterisations for passive tracers typically assume that eddy transport is both homogeneous and isotropic, but there is comprehensive evidence that eddy transport is in fact highly inhomogeneous and anisotropic (Berloff et al., 2002; Eden et al., 2007; Kamenkovich et al., 2009; Rypina et al., 2012; Kamenkovich et al., 2015; Bachman et al., 2020). For example, transport in eastward jets is highly anisotropic, with zonal eddy transport much greater than the meridional eddy transport due to meridional transport barriers on the jet core. On the jet flanks and beneath the jet, critical layers cause maxima in meridional transport, meaning there is significant cross-jet transport inhomogeneity (Ferrari and Nikurashin, 2010; Abernathey et al., 2010; Klocker and Abernathey, 2014). More generally, shear dispersion (Young et al., 1982; Jones and Young, 1994; Smith, 2005) leads to anisotropic transport being ubiquitous in the ocean. Many

parameterisations of eddy transport implement a scalar transfer co-efficient which cannot represent such anisotropy. For this reason the recent precursor studies Haigh et al. (2021a) and Haigh et al. (2021b), among others, make the case that transport tensors rather than scalar coefficients are more suitable for parameterising eddy tracer transport.

In this study we take a transport tensor approach, whereby an eddy tracer flux $\boldsymbol{f}$ is related to the large-scale tracer gradient $\nabla \overline{C}$ by the transport tensor $\boldsymbol{K}$ using the flux-gradient relation:

$$\boldsymbol{f} = -\boldsymbol{K} \nabla \overline{C}. \tag{1}$$

We diagnose the transport tensor from an eddy-resolving simulation, using a spatial filter to separate the large and small (eddy) scales. The diagnosed large- and small-scale flow and tracer fields are intended to represent the resolved and unresolved fields in non-eddy-resolving or eddy-permitting ocean models. For isopycnal transport $\boldsymbol{K}$ is a 2×2 tensor whose symmetric part $\boldsymbol{S}$ quantifies diffusive effects and whose antisymmetric part $\boldsymbol{A}$ quantifies advective effects. The diffusive flux $\boldsymbol{f}_{\text{diff}} = -\boldsymbol{S} \nabla \overline{C}$ affects the tracer variance (and all other moments apart from the mean (Griffies, 1998)) while the advective transport

---

* Corresponding author.
  E-mail address: m.haigh15@imperial.ac.uk (M. Haigh).

only 'stirs' the tracer and does not affect any moments. In this study we focus on the diffusive transport. The conceptual link to molecular diffusion and the requirement for simulations with parameterised eddy diffusion to be stable means authors usually seek positive (or non-negative) diffusion eigenvalues (Bachman et al., 2020). In this case the associated eddy tracer flux is never up-gradient, and always mixes the tracer by dissipating large-scale variance. Specifically, this means that the diffusive part of the eddy tracer flux drives a transfer of variance from the large (resolved) scales to the small (unresolved) scales.

Recent studies (Haigh et al., 2020; Stanley et al., 2020; Haigh et al., 2021a; Kamenkovich et al., 2021) have revealed that polar (opposite-sign) eigenvalues are a prevalent feature of the diagnosed diffusion tensor S for passive tracers. For polar eigenvalues the effects of the associated diffusive eddy tracer flux f_{diff} are not immediately clear. In general, for polar eigenvalues f_{diff} will drive filamentation of the tracer field, with f_{diff} being the sum of a down-gradient flux in the direction of the diffusion axis, that is the direction of preferential mixing, and an up-gradient flux perpendicular to this. When the diffusion axis is exactly parallel/perpendicular to $\nabla \overline{C}$, polar eigenvalues imply that the diffusive flux will be directly down-gradient/up-gradient, therefore having a diffusive/anti-diffusive effect. Thus, in the case of polar eigenvalues the direction of the variance transfer depends on the orientation of the diffusion axis relative to the orientation of the large-scale tracer gradient. One aim of this study is to determine the qualitative effects of the diffusive flux when the corresponding diffusion tensor has polar eigenvalues.

In ocean circulation models localised and transient up-gradient transfer is not necessarily an issue, but persistent up-gradient transfer could cause singularities to develop. Thus, care would have to be taken when parameterising diffusion tensors with any negative eigenvalues. To do this it is necessary to understand the effects of diffusion tensors with polar eigenvalues. In this study we diagnose eddy tracer fluxes, diffusion tensors and diffusion eigenvalues from an eddy-resolving quasigeostrophic simulation in which case the variance transfer effects of the diffusive eddy tracer flux are constrained by a stable ocean simulation with no development of singularities. Analysis of this diffusive eddy tracer flux can then inform future eddy transport parameterisations.

This study is organised as follows. In Section 2 we define the ocean model, the tracer model and the method for computing the eddy transport tensor. We also present the diffusion eigenvalues for two pairs of tracers. In Section 3 we define the variance budget for passive tracers and consider the domain-mean and time-mean balances. We then discuss how the variance transfer from the large scales to the small scales depends on relaxation of the tracer fields, and how the diffusion tensor accounts these dependencies. Lastly, in Section 4 we conclude and discuss our results.

2. The model

2.1. The ocean and tracer model

We consider passive tracers advected about a three-layer, square ocean basin ($x, y \in [0, L]$, $L = 3840$ km) by a lateral velocity field from a quasigeostrophic (QG) simulation. In each of the three layers the QG potential vorticity (PV) equation has the form

$$\frac{\partial q_k}{\partial t} + J(\psi_k, q_k) + \beta \frac{\partial \psi_k}{\partial x} = \nu \nabla^4 \psi_k - \delta_{3k} \gamma \nabla^2 \psi_k + \frac{\delta_{1k}}{\rho_1 H_1} W, \quad (2)$$

where $k = 1, 2, 3$ is the layer index. We also have: the beta-plane planetary vorticity gradient $\beta = 2 \times 10^{-11}$ m^{-1} s^{-1}; the eddy viscosity $\nu = 40$ m^2 s^{-1}; the bottom friction parameter $\gamma = 4 \times 10^{-8}$ s^{-1}; the upper-layer density $\rho_1 = 10^3$ kg m^{-3}; the mean layer thicknesses $H_1 = 250$ m, $H_2 = 750$ m and $H_3 = 3$ km. The asymmetric, tilted wind forcing W, used in numerous QG studies (e.g., Berloff, 2015; Haigh et al., 2020), is active only in the upper layer ($k = 1$), the bottom

friction is active only in the bottom layer, and both are controlled by the Kronecker delta δ_{ij}.

The Jacobian term $J(\psi_k, q_k)$ represents nonlinear advection of the QG PV anomalies q_k by the non-divergent lateral velocity $\boldsymbol{u}_k(x, y, t) = \hat{\boldsymbol{z}} \times \nabla \psi_k$ where ψ_k is the streamfunction and $\hat{\boldsymbol{z}}$ is the vertical unit vector. The streamfunctions and the PV anomalies are related via the elliptic equations,

$$q_1 = \nabla^2 \psi_1 + s_1(\psi_2 - \psi_1), \quad (3)$$

$$q_2 = \nabla^2 \psi_2 + s_{21}(\psi_1 - \psi_2) + s_{22}(\psi_3 - \psi_2), \quad (4)$$

$$q_3 = \nabla^2 \psi_3 + s_3(\psi_2 - \psi_3). \quad (5)$$

The stratification parameters, s_1, s_{21}, s_{22} and s_3, are defined such that the first and second Rossby deformation radii are 40 km and 20.6 km, respectively. The QG PV equations are simulated using the CABARET scheme (Karabasov et al., 2009) on a uniform 513^2 grid, corresponding to a resolution of 7.5 km. On the boundaries we use partial-slip conditions,

$$L_b \frac{\partial^2 \psi_k}{\partial n^2} - \frac{\partial \psi_k}{\partial n} = 0, \quad (6)$$

where $L_b = 120$ km is a boundary layer lengthscale and n is the coordinate normal to the boundary. Herein we will drop the layer index k for brevity, as all following equations are the same in each layer.

In each layer the evolution of a tracer $C(x, y, t)$ is governed by the advection–diffusion equation,

$$\frac{\partial C}{\partial t} + \nabla \cdot (\boldsymbol{u}C) = \nu \nabla^2 C + R. \quad (7)$$

We use the same value of the eddy viscosity $\nu = 40$ m^2 s^{-1} for the homogeneous subgrid diffusion of tracers. We will focus on two tracer pairs: one pair with nonlinear initial conditions, $C_{r1} = \sin(2\pi x/L)$, $C_{r2} = \sin(2\pi y/L)$, and one pair with linear initial conditions, $C_{r3} = x$, $C_{r4} = y$. In (7) R represents relaxation (Plumb and Mahlman, 1987) of the large-scale tracer field back to its initial condition:

$$R = r(C_r - \overline{C}), \quad (8)$$

for a relaxation rate r. We will focus on two cases: a strong relaxation case where $r = 1/5$ day^{-1} and a weak relaxation case where $r = 1/100$ day^{-1}. Here C_r is the tracer's initial condition/restoration field, and $\overline{C}(x, y, t)$ is the large-scale part of C. We use a spatial filter to obtain a field's large-scale part — the filter is formally defined in the next section. The QG and tracer simulations are spun up from rest until statistical equilibrium, after which we simulate the evolution for a further 2000 days with data saved daily. These 2000 days are deemed sufficient for the accumulated statistics presented in this study to have reached a steady state.

The purpose of the relaxation forcing is to maintain misalignment between the gradients of the tracers in each pair, which is necessary to accurately compute transport tensors for the pairs. The inclusion of relaxation can also be motivated by sources and sinks of many oceanic tracers. Typical examples include air–sea heat fluxes (Moore et al., 2012; Liang and Yu, 2016), air–sea exchange of tracers such as oxygen and carbon (Gruber et al., 2001; Gregg et al., 2014; Bushinsky et al., 2019), and precipitation and evaporation (Schmitt et al., 1989; Yu, 2019). These surface processes cause tracer sources/sinks with systematic large-scale spatial patterns leading to effects similar to a relaxation. At depth sources/sinks can be due to biogeochemical processes such as remineralisation and fixation of nitrate (Gruber and Sarmiento, 1997; Oschlies and Kähler, 2004; Eden and Oschlies, 2006). In our model the tracer evolution and the eddy tracer fluxes depend on the strength and spatial profile of the relaxation forcing, just as tracers and their eddy fluxes in ocean models depend on the sources/sinks (Wilson and Williams, 2006; Shuckburgh et al., 2011). The above-described processes are commonly implemented in the passive tracer component of ocean circulation models (e.g., Oschlies and Garçon (1998), Eden and Greatbatch (2009)). These models also include a standard down-gradient diffusion closure (Redi, 1982) to represent subgrid effects. It is the aim of this study to better inform parameterisations of subgrid effects in non-eddy-resolving and eddy-permitting ocean models.

2.2. Eddy transport

In this study we define eddies using a spatial filter (Nadiga, 2008; Fox-Kemper and Menemenlis, 2008; Lu et al., 2016; Bachman et al., 2017; Stanley et al., 2020). Given a discrete field snapshot ϕ_{ij}, where i, j denote the grid point in 2D space, the large-scale component is defined as

$$\overline{\phi}_{ij} = \frac{1}{w^2} \sum_{m=i-l}^{i+l} \sum_{n=j-l}^{j+l} \phi_{mn}, \quad \text{where} \quad l = \frac{w-1}{2}. \tag{9}$$

Here w is the odd filter width, which is reduced in size near the boundaries so that the filter remains square. The eddy field is $\phi'_{ij} = \phi_{ij} - \overline{\phi}_{ij}$. The spatial filter approach is a more suitable method than the temporal Reynolds decomposition for a number of reasons provided by Haigh et al. (2021a). In particular, in eddy-permitting ocean models, which are becoming more common given increasing computational power, there is no timescale separation between resolved and unresolved flows (Nadiga, 2008), meaning a temporal Reynolds eddy decomposition is not valid. In addition, our ability to resolve mesoscale eddies is limited by the spatial resolution, rather than temporal resolution, in which case a spatial filter is more suitable. We use a spatial filter with $w = 7$, corresponding to a physical filter side length of 45 km, slightly larger than the first deformation radius. This choice is best for targeting unresolved features of eddy-permitting ocean models, rather than entirely non-eddy-resolving models. We also computed our results for $w = 15$ and the conclusions made in this study apply in this case also. In our study we compute the large-scale and eddy velocity fields from the large-scale and eddy streamfunctions, rather than by directly decomposing the velocities. With this approach the 2D non-divergence of the velocities can be guaranteed for a general filter.

A common alternative to our square spatial filter is the Gaussian filter, but it is not known whether or not this option produces large-scale fields closer to the fields from a coarse-grid model. Alternatives to the standard spatial filtering have recently been developed by Agarwal et al. (2021) and Berloff et al. (2021). Agarwal et al. (2021) presented a method whereby the local dimensions of the filtering kernel are determined by local spatial correlations in the field being decomposed. Berloff et al. (2021) introduced the dynamical decomposition method via which, using eddy-resolving and non-eddy-resolving solutions, the exact eddy field missing from the non-eddy-resolving solution can be calculated. Both methods have been shown to lead to improved representations of mesoscale eddies and their effects. A worthwhile extension of the present study will therefore be to repeat the analysis using either of these two novel decomposition methods.

Filtering the tracer evolution equation yields the equation for the large-scale tracer field:

$$\frac{\partial \overline{C}}{\partial t} + \nabla \cdot (\overline{\boldsymbol{u}}\overline{C}) + \nabla \cdot \boldsymbol{f} = \nu \nabla^2 \overline{C} + \overline{R}, \tag{10}$$

where

$$\nabla \cdot \boldsymbol{f} = \overline{\nabla \cdot (\boldsymbol{u}C)} - \nabla \cdot (\overline{\boldsymbol{u}}\overline{C}) \tag{11}$$

is the divergence of the eddy tracer flux $\boldsymbol{f}$, which includes all eddy effects that are hypothetically not resolved in a coarse-grid simulation. Note that the filter operator commutes with the divergence operator everywhere except near the lateral boundaries.

Some authors Bachman et al. (2015, 2020) opt to work with the full eddy tracer flux. However, the rotational part of $\boldsymbol{f}$ typically dominates the divergent part by up two orders of magnitude Marshall and Shutts (1981), which was confirmed for the eddy fluxes of this model by Haigh et al. (2020). This means that inclusion of the rotational part of $\boldsymbol{f}$ will obscure analysis of its dynamically active divergent part, namely $\boldsymbol{f}_{\text{div}}$. In addition, because $\boldsymbol{f}$ is two orders of magnitude larger than $\boldsymbol{f}_{\text{div}}$, parameterising the latter is the safer option since any errors will be substantially less severe. For this reason we proceed with the divergent eddy tracer flux, as in recent studies (Haigh et al., 2021a,b; Kamenkovich et al., 2021). To obtain $\boldsymbol{f}_{\text{div}}$ we use the Helmholtz decomposition (Lau and Wallace, 1979) which separates a vector into divergent, rotational and harmonic parts. Specifically $\boldsymbol{f}_{\text{div}}$ is obtained by inverting the Poisson equation $\nabla^2 \phi = \nabla \cdot \boldsymbol{f}$ and then setting $\boldsymbol{f}_{\text{div}} = \nabla \phi$. The Helmholtz decomposition has a dependence on boundary conditions (Fox-Kemper et al., 2003); we use physically motivated zero normal flux boundary conditions (Maddison et al., 2015) that minimise the magnitude of $\boldsymbol{f}_{\text{div}}$. For brevity we will refer to $\boldsymbol{f}_{\text{div}}$ as just the eddy tracer flux.

In ocean circulation models the eddy tracer flux can be parameterised using a *transport tensor*:

$$\boldsymbol{f}_{\text{div}} = -\boldsymbol{K}\nabla \overline{C}. \tag{12}$$

The above equation, referred to as the flux-gradient relation, translates the need parameterise the eddy flux $\boldsymbol{f}_{\text{div}}$ into a need to parameterise the transport tensor $\boldsymbol{K}(x, y, t)$. This approach is motivated by classical parcel excursion theory (Taylor, 1921) in which, given a scale separation between the eddy and large scales, a Taylor expansion of the eddy flux predicts it is approximately proportional to the large-scale tracer gradient. Such a scale separation, either temporal or spatial, does not truly exist in the ocean, so use of a transport tensor in this way to quantify eddy tracer fluxes represents a somewhat ad hoc approach. An alternative is to parameterise the eddy tracer flux divergence directly, but unlike the flux-gradient approach this does not automatically guarantee conservation of tracer.

To invert the flux-gradient relation for $\boldsymbol{K}$ requires two tracers, or more if a least-squares approach were adopted (Bachman et al., 2015, 2020). In this study we compute $\boldsymbol{K}$ for a nonlinear tracer pair (restoration fields/initial conditions $C_{r1} = \sin(2\pi x/L)$, $C_{r2} = \sin(2\pi y/L)$) and linear tracer pair (restoration fields/initial conditions $C_{r3} = x$, $C_{r4} = y$). For a pair of tracers $C_p(x, y, t)$ and $C_q(x, y, t)$ with corresponding divergent eddy tracer fluxes $\boldsymbol{f}_p = (f_p^{(u)}, f_p^{(v)})$ and $\boldsymbol{f}_q = (f_q^{(u)}, f_q^{(v)})$, inverting (12) gives

$$\boldsymbol{K} \equiv \begin{pmatrix} K_{11} & K_{12} \\ K_{21} & K_{22} \end{pmatrix} = \frac{1}{d} \begin{pmatrix} f_p^{(u)} & f_q^{(u)} \\ f_p^{(v)} & f_q^{(v)} \end{pmatrix} \begin{pmatrix} -\overline{C}_{q,y} & \overline{C}_{q,x} \\ \overline{C}_{p,y} & -\overline{C}_{p,x} \end{pmatrix}, \tag{13}$$

where

$$d = \overline{C}_{p,x}\overline{C}_{q,y} - \overline{C}_{p,y}\overline{C}_{q,x} \tag{14}$$

is the determinant of the matrix of large-scale tracer gradients. In general $\boldsymbol{K}$ is non-unique meaning that it depends on the tracer pair used in the inversion, but this non-uniqueness is less severe once the rotational part of $\boldsymbol{f}$ is removed (Sun et al., 2021). Two reasons proposed for this non-uniqueness by Haigh et al. (2021a,b) are (i) incompleteness of the flux-gradient relation, meaning that $\boldsymbol{f}_{\text{div}}$ depends on the local tracer fields' curvature or history, and (ii) chaotic advection (Pierrehumbert, 1991), meaning that $\boldsymbol{K}$ is a stochastic object with a sensitive dependence on flow and tracer configurations. Note, though, because we remove the rotational part of $\boldsymbol{f}$, and because of the linearity of the flux-gradient relation and the tracer evolution equation, $\boldsymbol{K}$ is the same for all pairs of tracers with linear initial conditions/restorations fields.

We consider eddy transport with eddies defined using a spatial filter; Haigh et al. (2021a) compared $\boldsymbol{K}$ for spatial filter eddies with the transport tensor obtained for eddies defined using a temporal Reynolds decomposition. Despite the distinct scale separation method, many of the same processes will contribute to these different transport tensors. It was found that these transport tensors exhibit similar qualitative features, but with some significant differences, most notably near the eastward jet and western boundary current. A primary source of such differences are stationary eddies (Lu et al., 2016) which have small scales but persist in time and are common near the eastward jet and its meanders.

2.3. Eddy diffusion

The transport tensor K encompasses both diffusive and advective eddy effects, which can be separated by decomposing K into its symmetric and antisymmetric parts. We refer to the symmetric and antisymmetric parts as the *diffusion tensor* S and the *advection tensor* A, respectively. The physical difference between these tensors is that only the diffusion tensor and its associated diffusive flux $f_{\mathrm{diff}} = -S\nabla\overline{C}$ contribute to the variance transfer between the large and small scales. Such transfer is often referred to as 'mixing', with the implicit assumption that the transfer is down-gradient/down-scale. However, we will show that f_{diff} can often be up-gradient and has an anti-diffusive effect which contrasts the typical picture of f_{diff} being a strictly diffusive, i.e., strictly down-gradient, flux. The advection tensor and its associated skew flux[1] $f_{\mathrm{skew}} = -A\nabla\overline{C}$ only 'stir' the tracer (Griffies, 1998; Bachman et al., 2015), by which we mean that the transport does not affect the variance budget since the skew flux is perpendicular to the large-scale tracer gradient. Advective transport does, however, play an important role in the tracer redistribution and can enhance the gradients on which eddy diffusion and homogeneous diffusion act.

This study focuses on only the diffusive part of eddy transport, as is quantified by the diffusion tensor,

$$S = \frac{1}{2}\left(K + K^T\right). \tag{15}$$

Physical interpretation of S is aided by considering its eigenvalues and its principal axis, namely the *diffusion eigenvalues* and the *diffusion axis*, respectively. The diffusion axis v_1 represents the direction of preferential (down-gradient) diffusion, and its orientation is referred to as the *diffusion angle*, $\alpha \in [-\pi/2, \pi/2]$, where

$$\alpha = \frac{1}{2}\tan^{-1}\left(\frac{2S_{12}}{S_{11} - S_{22}}\right). \tag{16}$$

Given the diffusion angle, the diffusion eigenvalues are

$$\lambda_1 = S_{11}\cos^2\alpha + S_{22}\sin^2\alpha + 2S_{12}\cos\alpha\sin\alpha, \tag{17}$$

$$\lambda_2 = S_{11}\sin^2\alpha + S_{22}\cos^2\alpha - 2S_{12}\cos\alpha\sin\alpha. \tag{18}$$

If we ensure that α lies in the appropriate quadrant we guarantee that $\lambda_1 \geq \lambda_2$. In this case the diffusion axis $v_1 = (\cos\alpha, \sin\alpha)$ is the eigenvector corresponding to the most positive eigenvalue, λ_1. The second eigenvector $v_2 = (\sin\alpha, -\cos\alpha)$ is perpendicular to the first. With these definitions it can be shown that the diffusive flux is

$$f_{\mathrm{diff}} = -S\nabla\overline{C} = -|\nabla\overline{C}|\left(\lambda_1\cos(\alpha - \omega)v_1 + \lambda_2\sin(\alpha - \omega)v_2\right), \tag{19}$$

where ω is the orientation of the large-scale tracer gradient.

This study is motivated by the fact that opposite-signed, i.e., *polar*, eigenvalues have recently been diagnosed to be a prevalent feature of the diffusion tensor in both idealised QG simulations (Haigh et al., 2020, 2021a) and in comprehensive general circulation model simulations (Stanley et al., 2020; Kamenkovich et al., 2021). Haigh et al. (2020) and Haigh et al. (2021a) confirmed that polar eigenvalues were obtained for both a spatial filter scale separation and a temporal Reynolds decomposition. The expression (19) for the diffusive flux implies that with polar eigenvalues the diffusive flux is the sum of an up-gradient flux and a down-gradient flux, i.e., a truly diffusive flux and an anti-diffusive flux. The relative magnitudes of these fluxes is governed by the magnitudes of λ_1, λ_2 and the orientation of the diffusion axis v_1 relative to the large-scale tracer gradient $\nabla\overline{C}$. For example, when v_1 aligns with $\nabla\overline{C}$ only the λ_1 flux matters, while when v_1 and $\nabla\overline{C}$ are perpendicular only the λ_2 flux matters. In general, with polar eigenvalues the diffusive flux acts to stretch a tracer patch in the direction of the diffusion axis via the down-gradient flux

---

[1] Note the skew flux has the same divergence as the advective flux $f_{\mathrm{adv}} = u_*^c\overline{C}$, where u_*^c is an eddy-induced velocity whose streamfunction is the off-diagonal entry A_{21} of A (Griffies, 1998; Haigh et al., 2021b).

contribution, and compress the patch in the transverse direction via the up-gradient flux contribution. Any net up-gradient fluxes involved cannot persist indefinitely as this would lead to the development of singularities in the model. This of course does not occur in our stable tracer simulations, but the potential for such singularities to occur can motivate the consideration of only non-negative eigenvalues/diffusivities in parameterisations and diagnostics (Bachman et al., 2020).

In Fig. 1 we show 2D histograms of the diffusion eigenvalues for both the weak ($r = 1/100$ day^{-1}) and strong ($r = 1/5$ day^{-1}) relaxation cases for the nonlinear tracers C_1 and C_2. In Fig. 2 we show the same data but for the linear tracers C_3 and C_4. In each plot the data is accumulated over all grid points in the lower layer for 2000 days. (Throughout this study we will focus on the lower layer since here the statistics are least noisy and suffer least from alignment of tracer gradients. The weaker alignment is simply due to the flow being less vigorous at depth.) Firstly, the eigenvalue distributions depend on the tracer pair and the relaxation strength, with the tracer dependence amplified when the relaxation is stronger. For strong relaxation the eigenvalues are smaller in amplitude on average, most notably for the linear tracer pair. For both tracer pairs and relaxation strengths polar eigenvalues are most common, that is, compared to either pairs of negative or pairs of positive eigenvalues. Even though the eigenvalue distributions in Figs. 1 and 2 share this similarity, the diffusive nature of f_{diff} – that is, the extent to which it transfers variance from the large scales to the small scales – could be drastically different in each case.

Speaking more generally, we are yet to confirm that the diffusive flux in these simulations is even down-gradient, a 'desirable' property for a diffusive flux. In Fig. 3 we show histograms of the angle between the diffusive flux f_{diff} and the large-scale tracer gradient $\nabla\overline{C}$ in the lower layer for tracers C_1 and C_4. We choose these two tracers as they best illustrate the significant dependence that this angle has on the tracer restoration field and the relaxation amplitude. In some cases f_{diff} is most often oriented up-gradient (angles near zero), and almost as often down-gradient, whereas in other cases f_{diff} is most often oriented perpendicular to the tracer gradient. Such high frequencies of up-gradient eddy fluxes would be expected for active tracers such as momentum and PV (Haigh and Berloff, 2018, 2020), but may not be expected for passive tracers. For all tracers considered strengthening the relaxation increases the frequency of up-gradient fluxes. The extent of the diffusive or anti-diffusive effects of f_{diff} are determined by the amplitude of f_{diff} and $\nabla\overline{C}$ in addition to their relative orientation. To proceed we take these amplitudes into account in the context of the variance budget.

3. Eddy variance and variance transfer

3.1. The equations

Given a tracer field C and its large-scale part $\overline{C}$, we define the large-scale variance as $\Phi = \overline{C}^2/2$. The eddy variance (also often referred to as the subgrid-scale variance, residual variance or small-scale variance) is defined as $\phi = (\overline{C^2} - \overline{C}^2)/2$ (da Silva and Pereira, 2005). This can be interpreted as the sum of a covariance term $\overline{C}C'$ and an eddy-eddy variance term $(C')^2/2$. Some large-eddy simulation studies (Jiménez et al., 2001a,b; Balarac et al., 2008, 2013) define the eddy/subgrid scale variance as $\overline{\overline{C}^2} - \overline{\overline{C}}^2$, but these rely on the filter being a projection operator such that $\overline{C} = \overline{\overline{C}}$ (Cook and Riley, 1994; Cook et al., 1997). We opt to not impose this restriction on the spatial filter in this study, maintaining generality of our variance budget. For both our definition of the eddy variance $\phi = (\overline{C^2} - \overline{C}^2)/2$ and the alternative definition $\overline{\overline{C}^2} - \overline{\overline{C}}^2$ the role of the eddy tracer flux in the variance budget is exactly the same (aside from a factor of two). Therefore, the variance transfer and the dependence on relaxation is the same, meaning that the conclusions we make in this study do not depend on our precise definition of eddy variance.
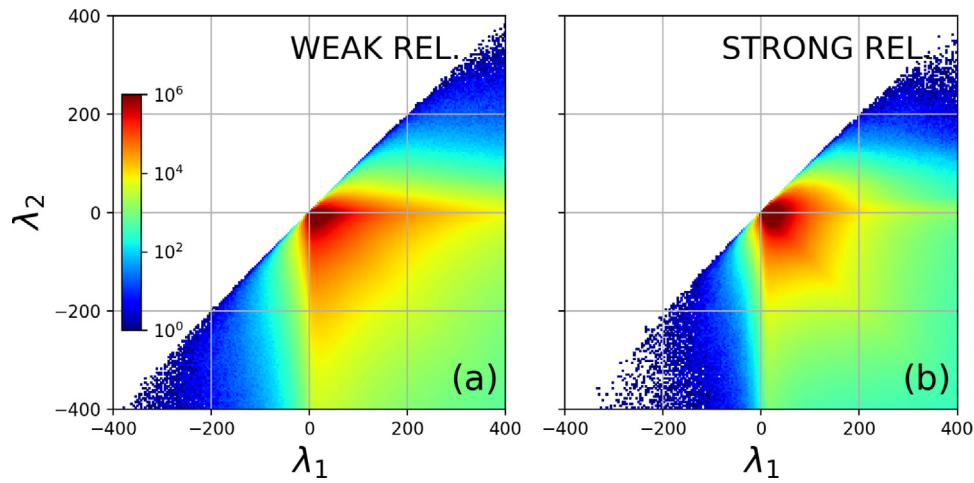
Fig. 1. 2D histograms of the two diffusion eigenvalues, λ_1 and λ_2, of the diffusion tensor for a pair of tracers with nonlinear restoration fields, $C_{r1} = \sin(2\pi x/L)$ and $C_{r2} = \sin(2\pi y/L)$. Panel (a) shows results for the case of weak relaxation and panel (b) is for the case of strong relaxation. Units on all axes are m^2 s^{-1}. The range for each eigenvalue is discretised into 200 bins. The colour represents the number of grid points whose eigenvalues lie in the bin, with data accumulated over 2000 days over all grid points in the lower layer.
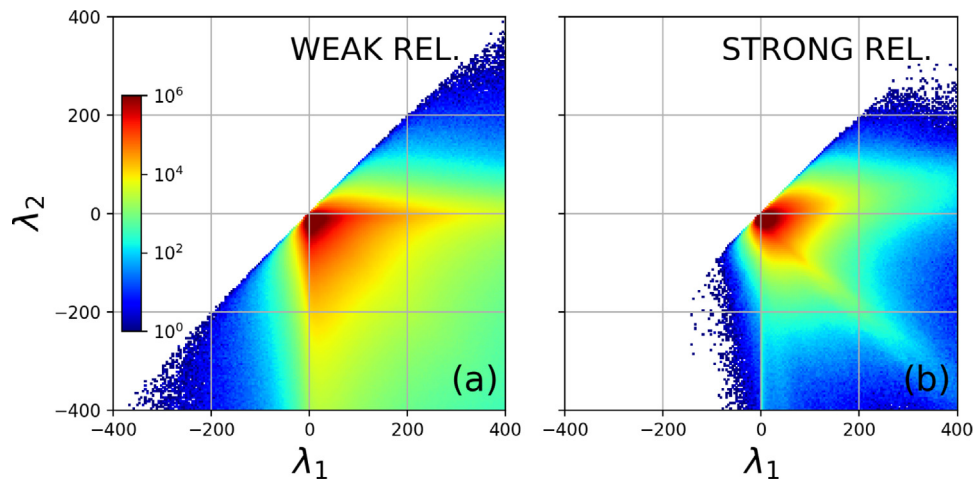
Fig. 2. 2D histograms of the two diffusion eigenvalues, λ_1 and λ_2, of the diffusion tensor for a pair of tracers with linear restoration fields, $C_{r3} = x$ and $C_{r4} = y$. Results are for (a) the weak relaxation case and (b) the strong relaxation case. All other details are the same as in Fig. 1.
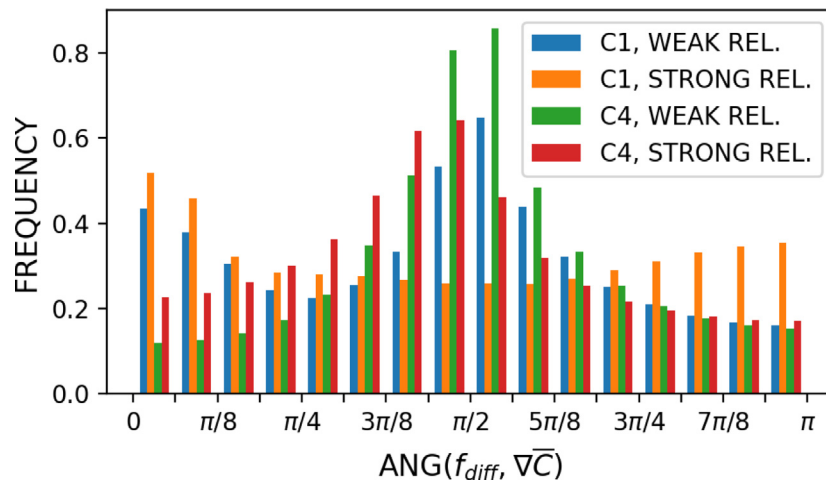
Fig. 3. Histograms of the angle between the diffusive flux f_{diff} and the large-scale tracer gradient $\nabla \overline{C}$ for tracers C_1 (blue, orange) and C_4 (green, red) in the lower layer. Results are for both weak (blue, green) and strong (orange, red) relaxation strengths.

Multiplying the large-scale tracer Eq. (10) by $\overline{C}$ yields the equation for the large-scale variance,

$$\frac{\partial \Phi}{\partial t} = F_\Phi + D_\Phi + R_\Phi + T_\Phi, \tag{20}$$

where

$$F_\Phi = -\nabla \cdot \left(\overline{\boldsymbol{u}} \Phi + \boldsymbol{f}_{\mathrm{div}} \overline{C} \right), \quad D_\Phi = \nu \overline{C} \, \overline{\nabla^2 C} \quad \text{and} \quad R_\Phi = \overline{C} \, \overline{R}. \tag{21}$$

Here F_Φ is the large-scale variance flux convergence, and D_Φ and R_Φ represent the effects on Φ due to dissipation and external forcing, respectively. Since the rotational part of the eddy tracer flux $\boldsymbol{f}$ does not affect the tracer evolution, it does not affect the variance budget. The variance transfer from the small scales to the large scales is

$$T_\Phi = \boldsymbol{f}_{\mathrm{div}} \cdot \nabla \overline{C} = \boldsymbol{f}_{\mathrm{diff}} \cdot \nabla \overline{C}. \tag{22}$$

Because the skew flux is perpendicular to $\nabla \overline{C}$ only the diffusive flux contributes to the transfer of variance between the scales. That only $\boldsymbol{f}_{\mathrm{diff}}$ contributes to the variance transfer is the defining quality of a diffusive flux. The equation for the eddy variance is

$$\frac{\partial \phi}{\partial t} = F_\phi + D_\phi + R_\phi + T_\phi, \tag{23}$$

where the eddy variance flux convergence (F_ϕ) and the effects of dissipation (D_ϕ) and external forcing (R_ϕ) on the eddy variance budget are

$$F_\phi = \nabla \cdot \left(\frac{1}{2} \left(\overline{\boldsymbol{u}} \overline{C}^2 - \overline{\boldsymbol{u} C^2} \right) + \boldsymbol{f}_{\mathrm{div}} \overline{C} \right), \quad D_\phi = \nu \overline{C \nabla^2 C} - \nu \overline{C} \, \overline{\nabla^2 C} \quad \text{and}$$

$$R_\phi = \overline{CR} - \overline{C} \, \overline{R}. \tag{24}$$

The transfer of variance from the large scales to the small scales is

$$T_\phi = -T_\Phi = -\boldsymbol{f}_{\mathrm{div}} \cdot \nabla \overline{C} = -\boldsymbol{f}_{\mathrm{diff}} \cdot \nabla \overline{C}. \tag{25}$$

Positive/negative T_ϕ implies an increase/decrease in ϕ and a decrease/increase in Φ.

In deriving our variance budget we have made no extra assumptions and have neglected no terms. Past studies often neglect a triple correlation term which represents advection of eddy variance by the eddy flow (Rhines and Holland, 1979; Marshall and Shutts, 1981), but Wilson and Williams (2004) have shown that this term is not negligible, just as it is not negligible in our budget. We also highlight that our variance budget includes no additional averaging, and applies for all time and space, unlike for the eddy variance budget with a Reynolds decomposition. Similarly, the variance transfer T_ϕ takes a similar form as when a Reynolds decomposition is used (Medvedev and Greatbatch, 2004; Wilson and Williams, 2004, 2006), but in our case the eddy tracer flux featuring in T_ϕ is contributed to by a number of terms and is not averaged.

3.2. The time-mean balance

In this section we present the time-mean eddy variance budget for the nonlinear tracer C_1, which has restoration field $C_{r1} = \sin(2\pi x/L)$. In Fig. 4 we show the time-mean (averaged over 2000 days) terms from the eddy variance budget F_ϕ, D_ϕ, R_ϕ, T_ϕ, for the case of weak relaxation $(1/r = 100$ days). In Fig. 5 we show the same data but for the case of strong relaxation $(1/r = 5$ days). Both examples are in the lower layer, but the main conclusions apply to all layers and all tracers considered.

Comparison of Figs. 4(a) and 5(a) indicates that the eddy variance flux convergence has a significant dependence on the relaxation strength, in addition to having a known dependence on the choice of tracer. For weaker relaxation F_ϕ is notably larger in magnitude, which is primarily due to the eddy tracer flux being larger in magnitude in this case, this being due to the weaker relaxation suppressing tracer field eddies less than strong relaxation does. Figs. 4(c) and 5(c) show that for both relaxation strengths in most of the domain we have down-gradient (diffusive) time-mean variance transfer, but smaller regions of weak up-gradient (anti-diffusive) time-mean transfer are also present.

For the case of strong relaxation, the relaxation term R_ϕ is the primary dissipator of eddy variance, while the effects of diffusion D_ϕ are an order of magnitude weaker. This is the case despite in some regions the relaxation acting to increase the eddy variance. These conclusions will be backed up in the next section. Importantly, although the relaxation is of the form $R = r(C_r - \overline{C})$, it still projects onto the eddy field because $(C_r - \overline{C})' \neq 0$. The effects of relaxation on the eddy variance budget are about half as strong in the weak relaxation case compared to the strong relaxation case, despite the relaxation rate being 20 times smaller in the former. The effects of homogeneous diffusion D_ϕ are an order of magnitude stronger in the case of weak relaxation compared to the case of strong relaxation. This is because, firstly, the weaker relaxation rate r means the difference $C_r - \overline{C}$ is larger so that the magnitude of the relaxation forcing $R = r \left(C_r - \overline{C} \right)$ does not decrease proportionally with r. Secondly, the weaker relaxation means that small-scale spatial variability is more weakly suppressed, causing the effects of homogeneous diffusion to be stronger than in the case of strong relaxation. Overall, this means that the net dissipation of eddy variance due to the relaxation and diffusion is stronger in the case of weak relaxation. This can only be compensated for by an increase in the transfer of variance from the large scales to the small scales as the relaxation weakens. This phenomena is evident when comparing Figs. 4(c) and 5(c), and will be demonstrated more completely for all tracers in the next section.

For eddies defined as the deviation from the time mean, Wilson and Williams (2006) found a strong positive correlation between the eddy variance transfer and the local advection of eddy variance. This led to the conclusion that a Lagrangian increase in tracer variance is associated with local down-gradient eddy fluxes. We do not observe any correlation (evaluated over all x, y, t, i.e., $513 \times 513 \times 2000$ data points) between F_ϕ and T_ϕ and still not for T_ϕ lagged behind F_ϕ (we tested lags from 0 to 50 days). Correlations between T_ϕ and R_ϕ may be useful as this would link up- and down-gradient fluxes to the relaxation, but we find no correlation between these terms. It is true, though, that positive T_ϕ typically occurs where R_ϕ is large and of any sign. We find a notable positive correlation (≈ 0.25) between T_ϕ and $|R_\phi|$ which is maximised when T_ϕ is lagged by 6 days behind R_ϕ. Wilson and Williams (2006) also concluded that local down-gradient fluxes can additionally be attributed to strong eddy variance dissipation (by eddy diffusion); our results agree with this finding since the time-mean down-gradient transfer is generally largest where the dissipation D_ϕ is largest, and time-mean up-gradient transfer occurs where D_ϕ is weak.

In the large-scale variance Φ budget (not shown) the dominant local balance is between the redistribution F_Φ and the forcing effects R_Φ. The spatial patterns of the eddy and large-scale variance budget terms depend on the tracer restoration field, but the dominant balances are the same for all four tracers that we consider. We only show spatial distributions of the eddy variance budget for tracer C_1 for brevity. To consider these in any more detail is out the scope of this study, and would require separate consideration of all tracers.

3.3. The domain-mean balance

The net transfer of variance from the large scales to the small scales is greater when relaxation is weaker, as is illustrated in Figs. 4(c) and 5(c) for tracer C_1. Although the spatial distributions of the variance budget terms depend on the tracer, this conclusion is true for all tracers considered and in all layers. To demonstrate this result further, we consider the domain-mean eddy variance budget. The domain-mean flux divergences of large-scale and eddy variance, F_Φ and F_ϕ, are zero since are both associated fluxes are zero through the boundaries. Thus, the steady-state, domain-mean balance for the large-scale and eddy variance budgets are

$$\tilde{D}_\Phi + \tilde{R}_\Phi + \tilde{T}_\Phi \approx 0 \quad \text{and} \quad \tilde{D}_\phi + \tilde{R}_\phi + \tilde{T}_\phi \approx 0, \tag{26}$$
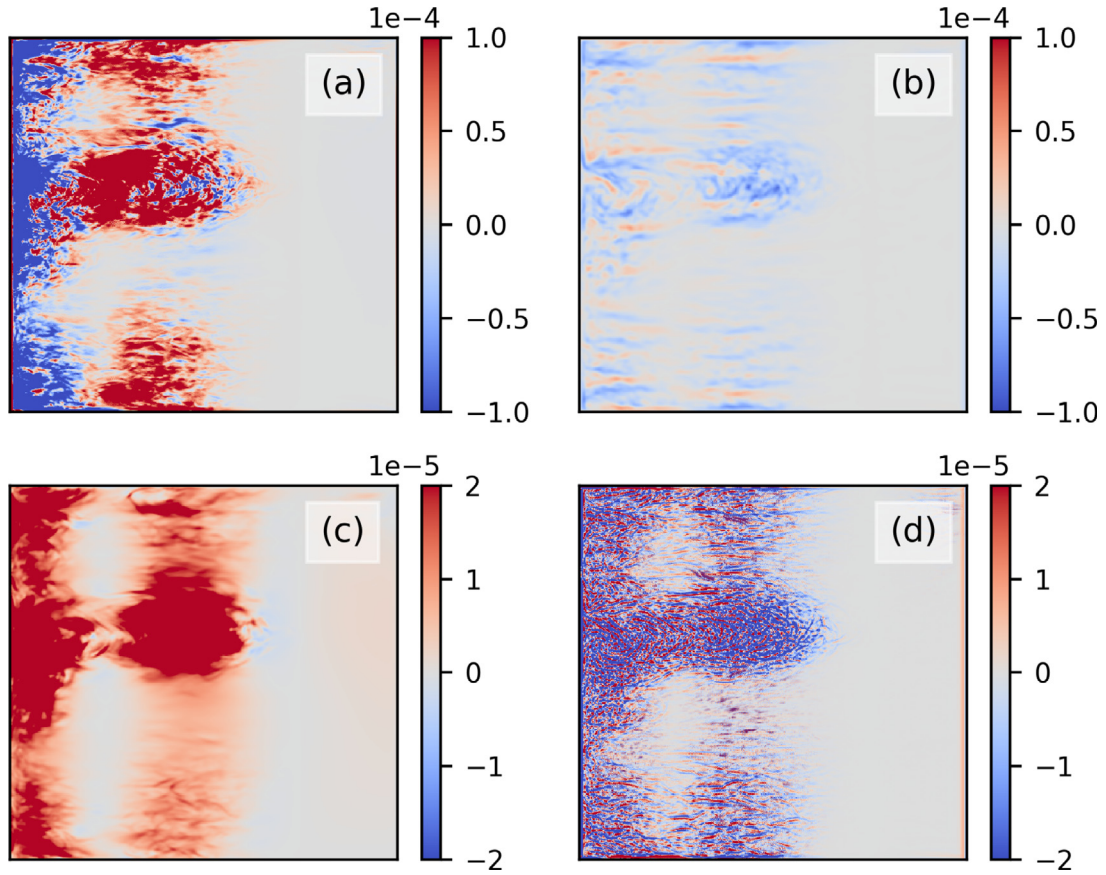
Fig. 4. The 2000-day time-mean terms (a) F_ϕ, (b) R_ϕ, (c) T_ϕ and (d) D_ϕ of the eddy variance budget for the case of weak relaxation ($1/r = 100$ days) and tracer C_1. Units are dimensionless. Panels (a) and (b) have colorbar ranges five times larger than panels (c) and (d).

where $\tilde{\cdot}$ denotes the domain mean. These state that when in equilibrium the transfer of variance at a given scale is approximately balanced by the effects of homogeneous diffusion and external forcing.

In Fig. 6 we show time series of $\tilde{T}_\phi$, $-\tilde{D}_\phi$ and $-\tilde{R}_\phi$ (note the minus signs) for both weak (upper panel) and strong (lower panel) relaxation. As before, these results are for tracer C_1 in the lower layer. Fig. 6 confirms that in both cases the integrated effect of the diffusive flux is to dissipate large-scale variance, i.e., transfer it down-gradient from the large scales to the small scales. For strong relaxation the eddy variance reduction due to the relaxation is predominantly balanced by the transfer from the large scales. For weak relaxation, the net variance reduction by $\tilde{R}_\phi$ only slightly decreases, while the net variance reduction by the diffusion term $\tilde{D}_\phi$ increases by a factor of 5. Therefore these time series confirm the result that there is an increase in total eddy variance dissipation when the relaxation is weaker, which must be compensated for by an increase in the down-gradient transfer of variance, $\tilde{T}_\phi$. We note, though, that the three terms $\tilde{T}_\phi$, $-\tilde{D}_\phi$ and $-\tilde{R}_\phi$ do not sum exactly to zero, which is due to temporal oscillations in the domain-mean eddy variance and small numerical errors induced by repeated filtering and differentiation.

In Fig. 7 we show time series of the domain-integrated transfer $\tilde{T}_\phi$ for tracers C_2, C_3 and C_4 for both relaxation strengths from which we make two conclusions. (1) For all tracers and both relaxation strengths the eddy tracer flux is on average down-gradient, since $\tilde{T}_\phi > 0$ in all cases. That is, even though the diffusion tensor has polar eigenvalues, the diffusive flux still has the 'desirable' effect of dissipating large-scale variance. (2) The net down-gradient transfer is greater when the relaxation is weaker for all tracers we consider. Although the diffusion eigenvalues are in general weaker for strong relaxation (Figs. 1 and 2), this is insufficient information to have made conclusion (2). This is because co-occurrences of negative diffusion eigenvalues are less likely

in the case of strong relaxation and because other factors, such as the diffusion axis and correlations between the diffusion axis, diffusion eigenvalues and the tracer gradients can also play an important role. We explore these factors in the next section.

3.4. The role of the diffusive flux and diffusion tensor

Polar eigenvalues are a prevalent feature of the diffusion tensor for both the weak and strong relaxation cases for both tracer pairs. We have shown, though, that for weaker relaxation the down-gradient variance transfer is stronger. This suggests that the diffusion axis is more likely to be oriented parallel to the tracer gradient when the relaxation is weaker. However, the variations in variance transfer could also be accounted for by the correlations between the diffusion axis, the diffusion eigenvalues and the tracer gradient. To explore this we return to the definition of the down-gradient variance transfer,

$$T_\phi = -T_\Phi = -\boldsymbol{f}_{\text{diff}} \cdot \nabla \overline{C}. \tag{27}$$

With Eq. (19) we showed that the diffusive flux can be expressed in terms of the diffusion eigenvalues λ_1, λ_2, the diffusion angle α and the tracer gradient amplitude $|\nabla \overline{C}|$ and orientation ω. Written in terms of the same quantities the variance transfer is

$$T_\phi = |\nabla \overline{C}|^2 \left[\lambda_1 \cos^2(\alpha - \omega) + \lambda_2 \sin^2(\alpha - \omega) \right]. \tag{28}$$

This equation confirms that when the diffusion axis and tracer gradient are parallel/perpendicular, only the first/second eigenvalue contributes to the transfer. This equation also illustrates how the eigenvalues are not the sole determinant of the variance transfer, and that $|\nabla \overline{C}|^2$ and $(\alpha - \omega)$ are important.

In Fig. 8 we show 2D histograms of (a) $|\nabla \overline{C}|^2 \lambda_1$ versus $\min(\alpha - \omega)$ and (b) $|\nabla \overline{C}|^2 \lambda_2$ versus $\min(\alpha - \omega)$ in the case of weak relaxation. We
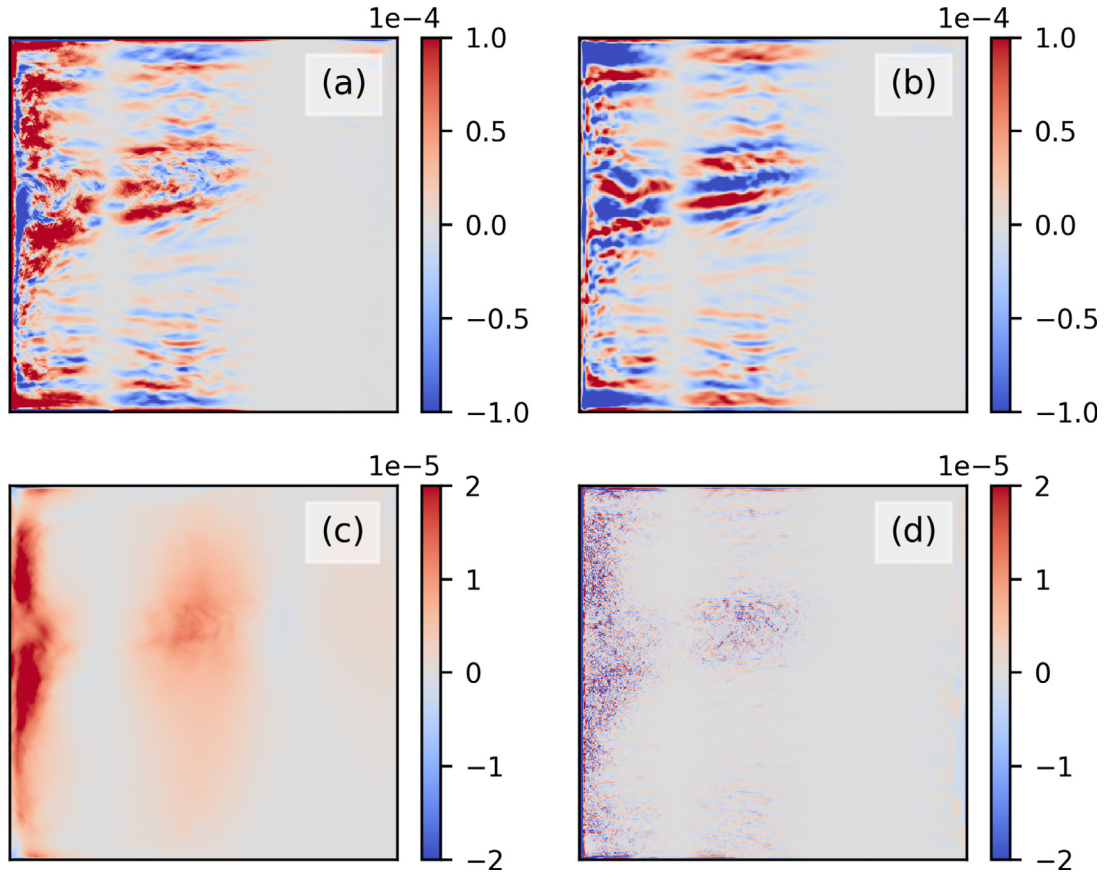
Fig. 5. The 2000-day time-mean terms (a) F_ϕ, (b) R_ϕ, (c) T_ϕ and (d) D_ϕ of the eddy variance budget for the case of strong relaxation ($1/r = 5$ days) and tracer C_1. The time-means of R_ϕ and D_ϕ both exhibited noisy spatial oscillations in the eastern fifth of the domain that appear when summing large contributions that mostly cancel. A filter was applied in the eastern fifth of the domain to reduce these oscillations. Panels (a) and (b) have colorbar ranges five times larger than panels (c) and (d).

scale the eigenvalues by $|\overline{\nabla C}|^2$ motivated by the prefactor in Eq. (28). The term $\min(\alpha - \omega)$ represents the smallest angle between the diffusion axis and the large-scale tracer gradient. In Fig. 9 we show the same data as in Fig. 8 but for the case of strong relaxation. Both figures are for tracer C_1 which has a nonlinear relaxation profile $C_{r1} = \sin(2\pi x/L)$. There are two important differences between the two pairs of distributions. First, the products $|\overline{\nabla C}|^2 \lambda_1$ and $|\overline{\nabla C}|^2 \lambda_2$ are on average larger in the case of weak relaxation — this is due to both the tracer gradient and the eigenvalues being stronger for weak relaxation. Second, for weak relaxation there is a notably higher frequency of positive and relatively large $|\overline{\nabla C}|^2 \lambda_2$ co-occurring with angle differences near $\pi/2$. Both of these account for the increased variance transfer in the weak relaxation case. For the other three tracers (results not shown) we make similar observations. We highlight, though, that for a given tracer pair the local diffusion axis cannot become more aligned (or more perpendicular) with both tracer gradients, since the two tracer gradients for a given tracer pair are close perpendicular in most instances. This means that the second observation, the relatively large $|\overline{\nabla C}|^2 \lambda_2$ co-occurring with angle differences near $\pi/2$, must be contributed to by different grid points for each tracer in a pair.

The conclusions we make in this section describe general trends which are not true at every grid point and instance in time. We can make the general conclusion, however, that the variations in variance transfer as the relaxation strength varies are accounted for by all properties of the diffusion tensor, i.e., the diffusion eigenvalues, the diffusion angle and correlations that these have with the large-scale tracer gradient. This notion adds to the apparent growing complexity (Kamenkovich et al., 2021) of the transport tensor for passive tracers. To move away from standard down-gradient eddy tracer transport parameterisations, and instead parameterise the highly complicated

transport/diffusion tensors that we diagnose represents a significant task. However, since polar eigenvalues, tracer filamentation, and co-existing diffusive and anti-diffusive eddy fluxes are such prevalent features of this eddy transport we argue that such an upgrade is necessary.

4. Conclusion

Recent studies have found that polar (opposite-signed) eigenvalues are a prevalent feature of the diffusion tensor for passive tracers in both idealised quasigeostrophic (QG) simulations (Haigh et al., 2020, 2021a) and general circulation model simulations (Stanley et al., 2020; Kamenkovich et al., 2021). Studies of polar diffusion eigenvalues, or any negative diffusivities, are scarce since simulations with parameterisations using negative diffusivities are more susceptible to instability issues. This has motivated some authors (Bachman et al., 2020) to use diagnostic methods that exclude negative diffusion eigenvalues. We argue that since polar eigenvalues are such a prevalent feature of diagnosed diffusion tensors, they require more research so that their associated tracer transport effects could eventually be incorporated into mesoscale eddy parameterisations.

In this study we categorised the mixing effects of eddy tracer fluxes whose associated diffusion tensors have polar eigenvalues by examining the variance transfer in an eddy-resolving QG simulation. We define eddies and the large scales using a spatial filter, akin to a large-eddy simulation (Fox-Kemper and Menemenlis, 2008; Nadiga, 2008) approach, but Haigh et al. (2020) and Haigh et al. (2021a) showed that polar eigenvalues were obtained for eddies defined using the more common temporal Reynolds decomposition. We considered two pairs of passive tracers, a 'linear' pair and a 'nonlinear' pair, and for each
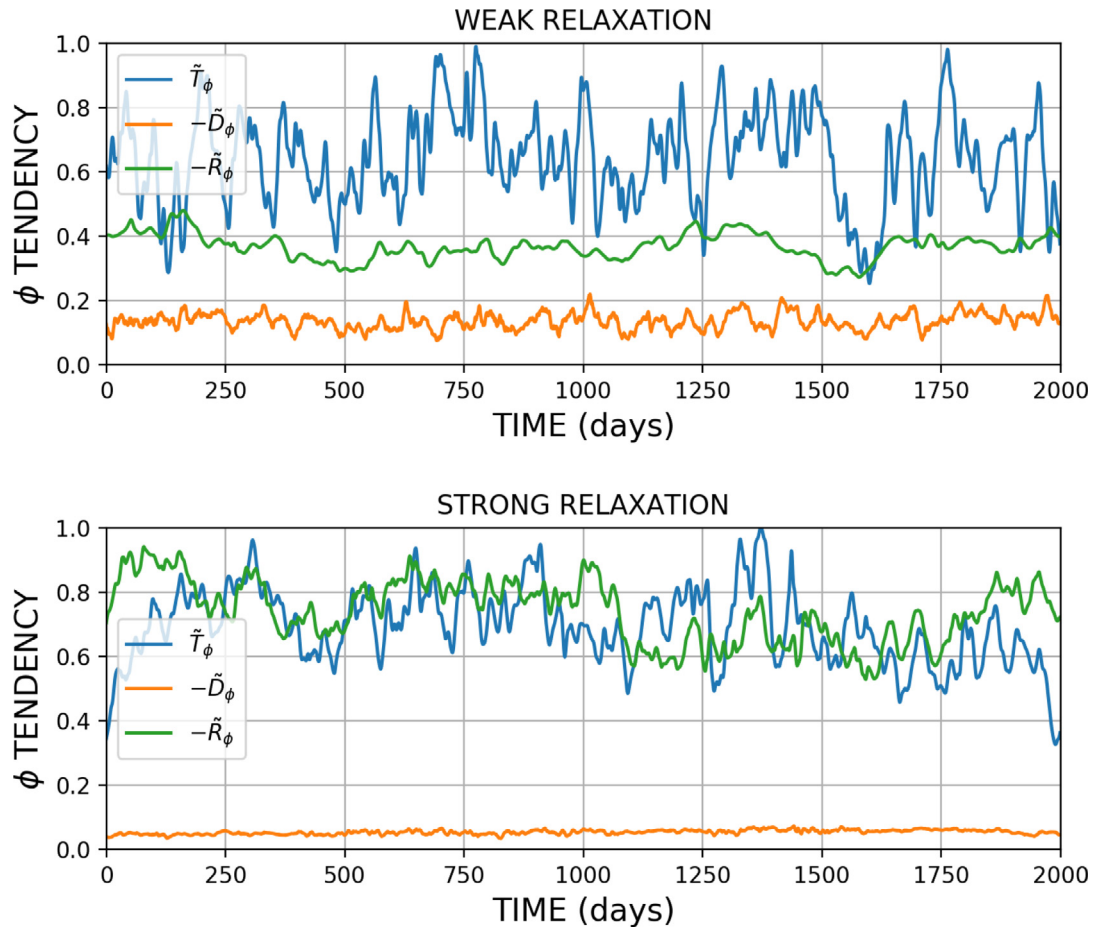
Fig. 6. Time series of the domain-mean terms in the eddy variance budget $\tilde{T}_\phi$, $-\tilde{D}_\phi$ and $-\tilde{R}_\phi$. These are for the case of weak relaxation (upper panel, $1/r = 100$ days) and strong relaxation (lower panel, $1/r = 5$ days) in the lower layer. Results are for tracer C_1. In each panel the time series are normalised by the maximum value of $\tilde{T}_\phi$. This value is roughly twice as large in the weak relaxation case compared to the strong relaxation case.
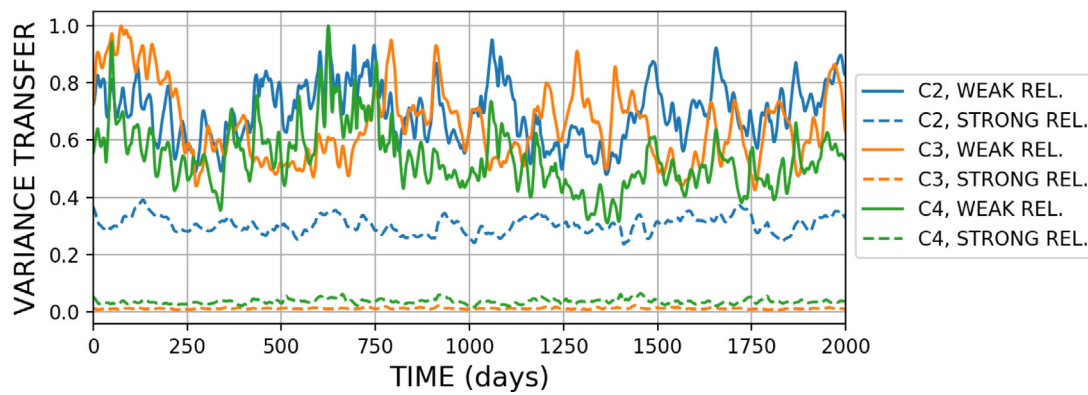
Fig. 7. Time series of domain-mean down-gradient variance transfer $\tilde{T}_\phi$ for tracers C_2, C_3 and C_4 for both relaxation strengths (see legend). The solid lines represent the weak relaxation cases and the dashed lines represent the strong relaxation cases. For each tracer its weak and strong relaxation $\tilde{T}_\phi$ time series are normalised by the maximum value of the weak relaxation time series.

pair the transport tensor and its symmetric part, the diffusion tensor, were obtained. In the tracer simulations the large-scale tracer components are relaxed towards the tracer initial condition, maintaining misalignment of tracer pairs, necessary for computing the transport tensors. The relaxation forcing can also be motivated by real-world tracer sources/sinks such as air–sea heat fluxes (Moore et al., 2012; Liang and Yu, 2016), air–sea exchange of oxygen and carbon (Gruber et al., 2001; Gregg et al., 2014; Bushinsky et al., 2019), precipitation and evaporation (Schmitt et al., 1989; Yu, 2019), and remineralisation and fixation of nitrate (Gruber and Sarmiento, 1997; Oschlies and

Kähler, 2004; Eden and Oschlies, 2006). We consider two relaxation strengths, a weak relaxation for which the relaxation timescale is 100 days, and a strong relaxation for which the timescale is 5 days. For each tracer pair and each relaxation strength the diffusion tensor is characterised by polar eigenvalues whose magnitudes are generally weaker in the strong relaxation case.

Polar eigenvalues in general parameterise fluxes that act to filament a tracer field (Ledwell et al., 1998), achieved by stretching a tracer patch in one direction and compressing it in the perpendicular direction. There is an additional dependence on the diffusion axis (the
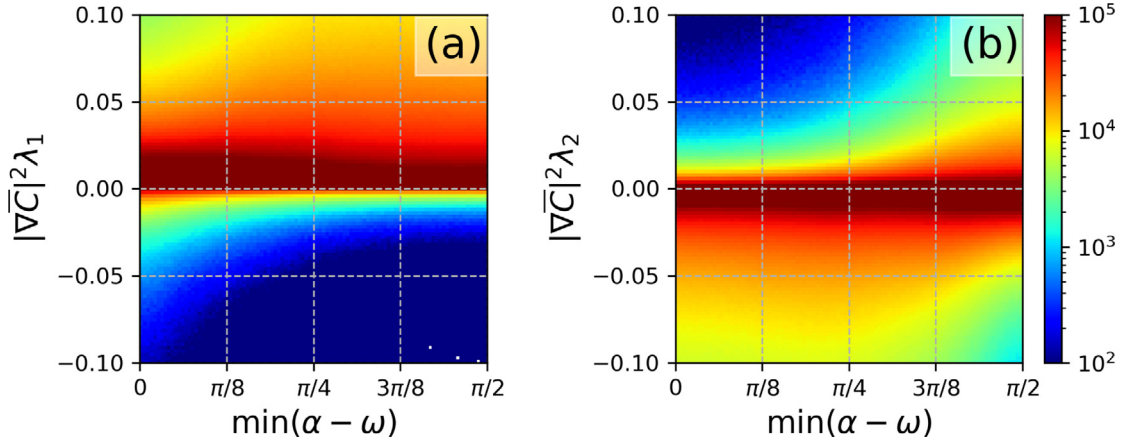
Fig. 8. Weak relaxation case. 2D histograms of (a) the scaled first diffusion eigenvalue $|\nabla \overline{C}|^2 \lambda_1$ and the angle difference $\alpha - \omega$ and (b) scaled second diffusion eigenvalue $|\nabla \overline{C}|^2 \lambda_2$ and the minimum angle difference $\alpha - \omega$. Results are for the lower layer and tracer C_1.
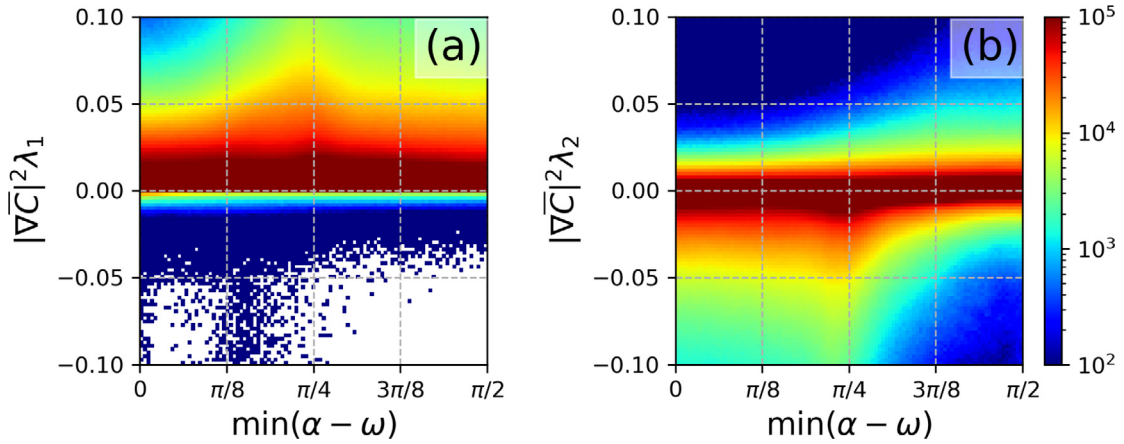
Fig. 9. The same as Fig. 8 but for the strong relaxation case.

principle axis of the diffusion tensor), such that polar eigenvalues can also quantify direct up- and down-gradient transfer. This means that for diffusion tensors with polar eigenvalues, the mixing effects of the diffusive eddy tracer flux, that is, the down-gradient transfer of variance that it drives, is not immediately clear. One of the main results of this study is that although the diffusion tensor has polar eigenvalues there is a net down-gradient transfer of variance for all tracers considered and both relaxation strengths. The eddy tracer flux therefore has the typically desirable effect of driving mixing, or more precisely dissipating large-scale variance, as would be guaranteed if both diffusion eigenvalues were positive. Locally up-gradient, i.e., anti-diffusive, fluxes are possible and for some tracers are more frequent (but weaker) than down-gradient ones. The location of these up-gradient fluxes strongly depends on the tracer and its relaxation profile; for each tracer we found a notable correlation (≈ 0.25) between the down-gradient variance transfer T_ϕ and the magnitude of the relaxation effects on the eddy variance budget $|R_\phi|$. Slightly larger correlations are found when T_ϕ is lagged 6 days behind $|R_\phi|$. These findings imply that strong down-gradient transfer is most common where $|R_\phi|$ is large, whereas up-gradient transfer is most common where $|R_\phi|$ is weak. A related finding is that the up-gradient fluxes are most persistent where the eddy variance dissipation is weakest, agreeing with the results of Wilson and Williams (2006).

The second main result is that as we weaken the relaxation strength, the net down-gradient transfer becomes markedly stronger, even though the prevalence of polar eigenvalues may not change, or that in the case of the linear tracers negative eigenvalues become more common. The variance transfer increases in this way because for weak relaxation the eddy field is more weakly suppressed, meaning that the

homogeneous diffusion has stronger small-scale gradients on which to act. The increased eddy variance dissipation by the homogeneous diffusion is only partly compensated for by a decrease in the dissipation by the relaxation forcing. Thus, an increase in down-gradient transfer as the relaxation weakens is required to maintain an approximate balance in the eddy variance budget. In the diffusion tensor this altered down-gradient transfer is jointly accounted for by the diffusion eigenvalues, the diffusion axis and the correlations that these have with the large-scale tracer gradient.

An important aim of any eddy transport parameterisation is to accurately emulate the transfer of variance between the resolved and unresolved scales (Jiménez et al., 2001a; Balarac et al., 2008, 2013; Lu and Porté-Agel, 2013). In this study we have shown that up-gradient fluxes and tracer filamentation are common features of eddy transport of passive tracers, but that down-gradient transfer remains the net effect. In contrast, current parameterisations of eddy tracer transport in ocean circulation models are strictly down-gradient. Our results therefore suggest that current parameterisations may require upgrading in order to accurately represent the tracer transport by mesoscale eddies missing in non-eddy-resolving and eddy-permitting ocean models. These models will simulate the evolution of tracers such as heat, salt, nitrate, oxygen and carbon (e.g., Eden and Oschlies (2006), Gregg et al. (2014)), each of which are forced by sources and sinks, and we have shown that such sources/sinks or relaxation effects can affect the nature of the eddy tracer transport. For example, persistent up-gradient fluxes are most common where the relaxation effects on the eddy variance budget are the weakest, a dependence which future parameterisations could aim to incorporate.

In our stable eddy-resolving tracer simulation advection and dissipation (by homogeneous diffusion and relaxation) of eddy variance prevent up-gradient fluxes from creating singularities. In a coarse-grid model with eddy transport parameterised, any prescribed negative diffusion eigenvalues may guarantee model instability. Future research must therefore focus on incorporating polar diffusion eigenvalue pairs into stable simulations by examining how other effects temper up-gradient fluxes in stable simulations. In a tracer transport model with polar eigenvalues it is sensible to retain a homogeneous down-gradient diffusion term to represent sub-mesoscale effects, such as those not resolved by the model we use in this study. Such a term will temper the effects of negative diffusion eigenvalues. Ensuring that negative diffusion eigenvalues are sufficiently transient or that the diffusion axis varies in time can also temper persistent up-gradient transfer and are known features of the diagnosed diffusion tensor. Lastly, it may be that the diffusion eigenvalues and diffusion angle have a precise relationship with the large-scale tracer field, accounted for by the non-uniqueness of K and S, which if somehow altered would cause the stable simulation to become unstable. Understanding this and the other processes that prevent up-gradient fluxes from causing singularities remains an important research extension.

CRediT authorship contribution statement

Michael Haigh: Conceptualisation, Methodology, Validation, Formal analysis, Investigation, Writing – original draft, Visualisation. **Pavel Berloff:** Software, Validation, Writing – review & editing, Supervision, Project administration, Funding acquisition.

Declaration of competing interest

The authors declare that they have no known competing financial interests or personal relationships that could have appeared to influence the work reported in this paper.

Acknowledgements

References

Abernathey, R., Marshall, J., Mazloff, M., Shuckburgh, E., 2010. Enhancement of mesoscale eddy stirring at steering levels in the southern ocean. J. Phys. Oceanogr. 40 (1), 170–184. http://dx.doi.org/10.1175/2009JPO4201.1.

Agarwal, N., Ryzhov, E.A., Kondrashov, D., Berloff, P., 2021. Correlation-based flow decomposition and statistical analysis of the eddy forcing. J. Fluid Mech. 924, A5. http://dx.doi.org/10.1017/jfm.2021.604.

Bachman, S.D., Fox-Kemper, B., Bryan, F.O., 2015. A tracer-based inversion method for diagnosing eddy-induced diffusivity and advection. Ocean Modell. (ISSN: 1463-5003) 86, 1–14. http://dx.doi.org/10.1016/j.ocemod.2014.11.006.

Bachman, S.D., Fox-Kemper, B., Bryan, F.O., 2020. A diagnosis of anisotropic eddy diffusion from a high-resolution global ocean model. J. Adv. Modelling Earth Syst. 12 (2), e2019MS001904. http://dx.doi.org/10.1029/2019MS001904.

Bachman, S.D., Fox-Kemper, B., Pearson, B., 2017. A scale-aware subgrid model for quasi-geostrophic turbulence. J. Geophys. Res. Oceans 122 (2), 1529–1554. http://dx.doi.org/10.1002/2016JC012265.

Balarac, G., Le Sommer, J., Meunier, X., Vollant, A., 2013. A dynamic regularized gradient model of the subgrid-scale scalar flux for large eddy simulations. Phys. Fluids 25 (7), 075107. http://dx.doi.org/10.1063/1.4813812.

Balarac, G., Pitsch, H., Raman, V., 2008. Development of a dynamic model for the subfilter scalar variance using the concept of optimal estimators. Phys. Fluids 20 (3), 035114. http://dx.doi.org/10.1063/1.2896287.

Berloff, P., 2015. Dynamically consistent parameterization of mesoscale eddies. Part I: Simple model. Ocean Model. (ISSN: 1463-5003) 87, 1–19. http://dx.doi.org/10.1016/j.ocemod.2014.12.008.

Berloff, P.S., McWilliams, J.C., Bracco, A., 2002. Material transport in oceanic gyres. Part I: Phenomenology. J. Phys. Oceanogr. 32 (3), 764–796. http://dx.doi.org/10.1175/1520-0485(2002)032<0764:MTIOGP>2.0.CO;2.

Berloff, P., Ryzhov, E., Shevchenko, I., 2021. On dynamically unresolved oceanic mesoscale motions. J. Fluid Mech. 920, A41. http://dx.doi.org/10.1017/jfm.2021.477.

Bushinsky, S.M., Landschützer, P., Rödenbeck, C., Gray, A.R., Baker, D., Mazloff, M.R., Resplandy, L., Johnson, K.S., Sarmiento, J.L., 2019. Reassessing southern ocean air-sea CO2 flux estimates with the addition of biogeochemical float observations. Glob. Biogeochem. Cycles 33 (11), 1370–1388. http://dx.doi.org/10.1029/2019GB006176.

Cook, A.W., Riley, J.J., 1994. A subgrid model for equilibrium chemistry in turbulent flows. Phys. Fluids 6 (8), 2868–2870. http://dx.doi.org/10.1063/1.868111.

Cook, A.W., Riley, J.J., Kosály, G., 1997. A laminar flamelet approach to subgrid-scale chemistry in turbulent flows. Combust. Flame (ISSN: 0010-2180) 109 (3), 332–341. http://dx.doi.org/10.1016/S0010-2180(97)83066-0.

da Silva, C.B., Pereira, J.C.F., 2005. On the local equilibrium of the subgrid scales: The velocity and scalar fields. Phys. Fluids 17 (10), 108103. http://dx.doi.org/10.1063/1.2104747.

Eden, C., Greatbatch, R.J., 2009. A diagnosis of isopycnal mixing by mesoscale eddies. Ocean Modell. (ISSN: 1463-5003) 27 (1), 98–106. http://dx.doi.org/10.1016/j.ocemod.2008.12.002.

Eden, C., Greatbatch, R.J., Olbers, D., 2007. Interpreting eddy fluxes. J. Phys. Oceanogr. 37 (5), 1282–1296. http://dx.doi.org/10.1175/JPO3050.1.

Eden, C., Oschlies, A., 2006. Adiabatic reduction of circulation-related CO2 air-sea flux biases in a north atlantic carbon-cycle model. Glob. Biogeochem. Cycles 20 (2), http://dx.doi.org/10.1029/2005GB002521.

Ferrari, R., Nikurashin, M., 2010. Suppression of eddy diffusivity across jets in the southern ocean. J. Phys. Oceanogr. 40 (7), 1501–1519. http://dx.doi.org/10.1175/2010JPO4278.1.

Fox-Kemper, B., Ferrari, R., Pedlosky, J., 2003. On the indeterminacy of rotational and divergent eddy fluxes. J. Phys. Oceanogr. 33 (2), 478–483. http://dx.doi.org/10.1175/1520-0485(2003)033<0478:OTIORA>2.0.CO;2.

Fox-Kemper, B., Menemenlis, D., 2008. Can large eddy simulation techniques improve mesoscale rich ocean models? In: Ocean Modeling in an Eddying Regime. American Geophysical Union (AGU), ISBN: 9781118666432, pp. 319–337. http://dx.doi.org/10.1029/177GM19.

Gregg, W.W., Casey, N.W., Rousseaux, C.S., 2014. Sensitivity of simulated global ocean carbon flux estimates to forcing by reanalysis products. Ocean Model. (ISSN: 1463-5003) 80, 24–35. http://dx.doi.org/10.1016/j.ocemod.2014.05.002.

Griffies, S.M., 1998. The Gent–Mcwilliams skew flux. J. Phys. Oceanogr. 28 (5), 831–841. http://dx.doi.org/10.1175/1520-0485(1998)028<0831:TGMSF>2.0.CO;2.

Gruber, N., Gloor, M., Fan, S.-M., Sarmiento, J.L., 2001. Air-sea flux of oxygen estimated from bulk data: Implications for the marine and atmospheric oxygen cycles. Glob. Biogeochem. Cycles 15 (4), 783–803. http://dx.doi.org/10.1029/2000GB001302.

Gruber, N., Sarmiento, J.L., 1997. Global patterns of marine nitrogen fixation and denitrification. Glob. Biogeochem. Cycles 11 (2), 235–266. http://dx.doi.org/10.1029/97GB00077.

Haigh, M.C., Berloff, P.S., 2018. Potential vorticity redistribution by localised transient forcing in the shallow-water model. J. Fluid Mech. 852, 199–225. http://dx.doi.org/10.1017/jfm.2018.547.

Haigh, M., Berloff, P., 2020. Rossby waves and zonal momentum redistribution induced by localised forcing in the rotating shallow-water model. J. Fluid Mech. 885, A43. http://dx.doi.org/10.1017/jfm.2019.1032.

Haigh, M., Sun, L., McWilliams, J.C., Berloff, P., 2021a. On eddy transport in the ocean. Part I: The diffusion tensor. Ocean Modell. (ISSN: 1463-5003) 164, 101831. http://dx.doi.org/10.1016/j.ocemod.2021.101831.

Haigh, M., Sun, L., McWilliams, J.C., Berloff, P., 2021b. On eddy transport in the ocean. Part II: The advection tensor. Ocean Model. (ISSN: 1463-5003) 165, 101845. http://dx.doi.org/10.1016/j.ocemod.2021.101845.

Haigh, M., Sun, L., Shevchenko, I., Berloff, P., 2020. Tracer-based estimates of eddy-induced diffusivities. Deep Sea Res. I (ISSN: 0967-0637) http://dx.doi.org/10.1016/j.dsr.2020.103264.

Jiménez, C., Ducros, F., Cuenot, B., Bédat, B., 2001a. Subgrid scale variance and dissipation of a scalar field in large eddy simulations. Phys. Fluids 13 (6), 1748–1754. http://dx.doi.org/10.1063/1.1366668.

Jiménez, C., Valiño, L., Dopazo, C., 2001b. A priori and a posteriori tests of subgrid scale models for scalar transport. Phys. Fluids 13 (8), 2433–2436. http://dx.doi.org/10.1063/1.1384891.

Jones, S.W., Young, W.R., 1994. Shear dispersion and anomalous diffusion by chaotic advection. J. Fluid Mech. 280, 149–172. http://dx.doi.org/10.1017/S0022112094002880.

Kamenkovich, I., Berloff, P., Haigh, M., Sun, L., Lu, Y., 2021. Complexity of mesoscale eddy diffusivity in the ocean. Geophys. Res. Lett. 45 (3), e2020GL091719. http://dx.doi.org/10.1029/2020GL091719, e2020GL091719 2020GL091719.

Kamenkovich, I., Berloff, P.S., Pedlosky, J., 2009. Anisotropic material transport by eddies and eddy-driven currents in a model of the North Atlantic. J. Phys. Oceanogr. (ISSN: 0022-3670) 39 (12), 3162–3175. http://dx.doi.org/10.1175/2009JPO4239.1.

Kamenkovich, I., Rypina, I.I., Berloff, P.S., 2015. Properties and origins of the anisotropic eddy-induced transport in the North Atlantic. J. Phys. Oceanogr. 45 (3), 778–791. http://dx.doi.org/10.1175/JPO-D-14-0164.1.

Karabasov, S.A., Berloff, P.S., Goloviznin, V.M., 2009. CABARET in the ocean gyres. Ocean Modell. (ISSN: 1463-5003) 30 (2), 155–168. http://dx.doi.org/10.1016/j.ocemod.2009.06.009.

Klocker, A., Abernathey, R., 2014. Global patterns of mesoscale eddy properties and diffusivities. J. Phys. Oceanogr. 44 (3), 1030–1046. http://dx.doi.org/10.1175/JPO-D-13-0159.1.

Lau, N.C., Wallace, John M., 1979. On the distribution of horizontal transports by transient eddies in the northern hemisphere wintertime circulation'. J. Atmospheric Sciences 36 (10), 1844–1861. http://dx.doi.org/10.1175/1520-0469(1979)036<1844:OTDOHT>2.0.CO;2.

Ledwell, J.R., Watson, A.J., Law, C.S., 1998. Mixing of a tracer in the pycnocline. J. Geophys. Res. Oceans (ISSN: 0148-0227) 103 (C10), 21499–21529. http://dx.doi.org/10.1029/98JC01738.

Liang, X., Yu, L., 2016. Variations of the global net air–sea heat flux during the "hiatus" period (2001–10). J. Clim. 29 (10), 3647–3660. http://dx.doi.org/10.1175/JCLI-D-15-0626.1.

Lu, H., Porté-Agel, F., 2013. A modulated gradient model for scalar transport in large-eddy simulation of the atmospheric boundary layer. Phys. Fluids 25 (1), 015110. http://dx.doi.org/10.1063/1.4774342.

Lu, J., Wang, F., Liu, H., Lin, P., 2016. Stationary mesoscale eddies, upgradient eddy fluxes, and the anisotropy of eddy diffusivity. Geophys. Res. Lett. 43 (2), 743–751. http://dx.doi.org/10.1002/2015GL067384.

Maddison, J.R., Marshall, D.P., Shipton, J., 2015. On the dynamical influence of ocean eddy potential vorticity fluxes. Ocean Modell. (ISSN: 1463-5003) 92, 169–182. http://dx.doi.org/10.1016/j.ocemod.2015.06.003.

Marshall, J., Shutts, G., 1981. A note on rotational and divergent eddy fluxes. J. Phys. Oceanogr. 11 (12), 1677–1680. http://dx.doi.org/10.1175/1520-0485(1981)011<1677:ANORAD>2.0.CO;2.

Medvedev, A.S., Greatbatch, R.J., 2004. On advection and diffusion in the mesosphere and lower thermosphere: The role of rotational fluxes. J. Geophys. Res.: Atmos. 109 (D7), http://dx.doi.org/10.1029/2003JD003931.

Moore, G.W.K., Renfrew, I.A., Pickart, R.S., 2012. Spatial distribution of air-sea heat fluxes over the sub-polar north atlantic ocean. Geophys. Res. Lett. 39 (18), http://dx.doi.org/10.1029/2012GL053097.

Nadiga, B.T., 2008. Orientation of eddy fluxes in geostrophic turbulence. Phil. Trans. R. Soc. A 366 (1875), 2489–2508. http://dx.doi.org/10.1098/rsta.2008.0058.

Oschlies, A., Garçon, V., 1998. Eddy-induced enhancement of primary production in a model of the North Atlantic Ocean. Nature 394 (6690), 266–269. http://dx.doi.org/10.1038/28373,

Oschlies, A., Kähler, P., 2004. Biotic contribution to air-sea fluxes of CO2 and O2 and its relation to new production, export production, and net community production. Glob. Biogeochem. Cycles 18 (1), http://dx.doi.org/10.1029/2003GB002094.

Pierrehumbert, R.T., 1991. Chaotic mixing of tracer and vorticity by modulated travelling rossby waves. Geophys. Astrophys. Fluid Dyn. 58 (1–4), 285–319. http://dx.doi.org/10.1080/03091929108227343.

Plumb, R., Mahlman, J., 1987. The zonally averaged transport characteristics of the GFDL general circulation/transport model. J. Atmos. Sci. 44, 298–327. http://dx.doi.org/10.1175/1520-0469(1987)044<0298:TZATCO>2.0.CO;2.

Redi, M.H., 1982. Oceanic isopycnal mixing by coordinate rotation. J. Phys. Oceanogr. (ISSN: 0022-3670) 12 (10), 1154–1158. http://dx.doi.org/10.1175/1520-0485(1982)012<1154:OIMBCR>2.0.CO;2.

Rhines, P.B., Holland, W.R., 1979. A theoretical discussion of eddy-driven mean flows. Dyn. Atmos. Oceans (ISSN: 0377-0265) 3 (2), 289–325. http://dx.doi.org/10.1016/0377-0265(79)90015-0.

Rypina, I.I., Kamenkovich, I., Berloff, P.S., Pratt, L.J., 2012. Eddy-induced particle dispersion in the near-surface North Atlantic. J. Phys. Oceanogr. 42 (12), 2206–2228. http://dx.doi.org/10.1175/JPO-D-11-0191.1.

Schmitt, R.W., Bogden, P.S., Dorman, C.E., 1989. Evaporation minus precipitation and density fluxes for the North Atlantic. J. Phys. Oceanogr. 19 (9), 1208–1221. http://dx.doi.org/10.1175/1520-0485(1989)019<1208:EMPADF>2.0.CO;2.

Shuckburgh, E., Maze, G., Ferreira, D., Marshall, J., Jones, H., Hill, C., 2011. Mixed layer lateral eddy fluxes mediated by air-sea interaction. J. Phys. Oceanogr. 41 (1), 130–144. http://dx.doi.org/10.1175/2010JPO4429.1.

Smith, K.S., 2005. Tracer transport along and across coherent jets in two-dimensional turbulent flow. J. Fluid Mech. 544, 133–142. http://dx.doi.org/10.1017/S0022112005006750.

Stanley, Z., Bachman, S.D., Grooms, I., 2020. Vertical structure of ocean mesoscale eddies with implications for parameterizations of tracer transport. J. Adv. Modelling Earth Syst. 12 (10), e2020MS002151. http://dx.doi.org/10.1029/2020MS002151.

Sun, L., Haigh, M., Shevchenko, I., Berloff, P., Kamenkovich, I., 2021. On non-uniqueness of the mesoscale eddy diffusivity. J. Fluid Mech. 920, A32. http://dx.doi.org/10.1017/jfm.2021.472.

Taylor, G.I., 1921. Diffusion by continuous movements. Proc. Lond. Math. Soc. s2-20 (1), 196–212. http://dx.doi.org/10.1112/plms/s2-20.1.196.

Wilson, C., Williams, R.G., 2004. Why are eddy fluxes of potential vorticity difficult to parameterize? J. Phys. Oceanogr. 34 (1), 142–155. http://dx.doi.org/10.1175/1520-0485(2004)034<0142:WAEFOP>2.0.CO;2.

Wilson, C., Williams, R.G., 2006. When are eddy tracer fluxes directed downgradient? J. Phys. Oceanogr. 36 (2), 189–201. http://dx.doi.org/10.1175/JPO2841.1.

Young, W.R., Rhines, P.B., Garrett, C.J.R., 1982. Shear-flow dispersion, internal waves and horizontal mixing in the ocean. J. Phys. Oceanogr. 12 (6), 515–527. http://dx.doi.org/10.1175/1520-0485(1982)012<0515:SFDIWA>2.0.CO;2.

Yu, L., 2019. Global air–sea fluxes of heat, fresh water, and momentum: Energy budget closure and unanswered questions. Annual Rev. Mar. Sci. 11 (1), 227–248. http://dx.doi.org/10.1146/annurev-marine-010816-060704, PMID: 30156969.